Synthetic-Space Photonic Topological Insulators Utilizing Dynamically Invariant Structure

Liat Nemirovsky, Moshe-Ishay Cohen, Yaakov Lumer, Eran Lustig, and Mordechai Segev*
Solid State Institute, and Department of Physics, Technion-Israel Institute of Technology, Haifa 32000, Israel

(Received 14 September 2020; accepted 1 July 2021; published 25 August 2021)

Synthetic-space topological insulators are topological systems with at least one spatial dimension replaced by a periodic arrangement of modes, in the form of a ladder of energy levels, cavity modes, or some other sequence of modes. Such systems can significantly enrich the physics of topological insulators, in facilitating higher dimensions, nonlocal coupling, and more. Thus far, all synthetic-space topological insulators relied on active modulation to facilitate transport in the synthetic dimensions. Here, we propose dynamically invariant synthetic-space photonic topological insulators: a two-dimensional evolution-invariant photonic structure exhibiting topological properties in synthetic dimensions. This nonmagnetic structure is static, lacking any kind of modulation in the evolution coordinate, yet it displays an effective magnetic field in synthetic space, characterized by a Chern number of one. We study the evolution of topological states along the edge, and on the interface between two such structures with opposite synthetic-space chirality, and demonstrate their robust unidirectional propagation in the presence of defects and disorder. Such topological structures can be realized in photonics and cold atoms and provide a fundamentally new mechanism for topological insulators.

DOI: 10.1103/PhysRevLett.127.093901

Topological insulators (TIs) [1] attract an abundance of research in many different fields. These materials are insulators in the bulk but perfectly conduct on the edge. Their edge states are defined by discrete topological invariants, and their transport is robust against disorder if the topological band gap is large enough. In the past decade, TIs were demonstrated in a variety of systems such as electronics [2], microwaves [3], photonics [4–9], cold atoms [10,11], acoustics [12,13], and mechanics [14,15]. The major progress with topological phenomena in electromagnetic (EM) waves has led to the new field of topological photonics [16], enabled exploring the physics of topological systems in settings that are impossible in solid state physics [17], and offered novel contexts, such as nonreciprocal EM devices [3], radiation-free sharply bent waveguides [18], and an avenue to force many semiconductor lasers to lock and act as a single laser source [19].

TIs usually rely on spatial lattices, with the wave packets therein subjected to gauge fields that give rise to the topological phenomena. However, lattices do not necessarily have to be a spatial arrangement of sites. Rather, a lattice can also be ladders of atomic states [20–23], cavity modes [24–27], waveguide array modes [28], judiciously interconnected photonic systems [29–32], or the states arising from shaking harmonic traps [33] (See recent review on topological photonics in synthetic dimensions [34]). In this vein, spatial lattices can be augmented by one or more synthetic dimensions. With this concept, one can engineer geometries with gauge fields that are not available in spatial lattices [35] and produce lattices with unusual features such as topologically protected states in the real-space bulk [28], protected transport utilizing the frequency domain as the synthetic dimension [24,27], or inducing an artificial magnetic field which does not break time-reversal symmetry in real-space [36]. In addition, synthetic dimensions enable one to explore physics in a space with a dimensionality higher than the apparent geometrical dimension of these structures [28,37]. This concept provides a promising basis for new topological photonic structures, such as a mode-locked topological insulator laser [38]. However, thus far, all suggestions and experiments on photonic topological insulators (PTIs) in synthetic dimensions relied on modulation to couple the modes and facilitate transport in the synthetic dimensions. Such modulation has to be in the evolution dimension and can be either in time [24,25] or along the propagation dimension [28].

Here, we propose synthetic-space PTIs relying on dynamically invariant topological photonic structure. This structure is the first evolution-invariant system which is a synthetic-space TI [36]. We show that this structure is characterized by a real-space Chern number of $+1$ and demonstrate robust one-way edge propagation in synthetic dimensions without breaking time-reversal symmetry in real-space.

Creating nonmagnetic PTIs that do not require any modulation, neither in time nor along the propagation axis, is valuable, because these systems do not involve coupling to unbound states (which inevitably introduce loss) [39]. For example, in Ref. [4], the helicity of the waveguides

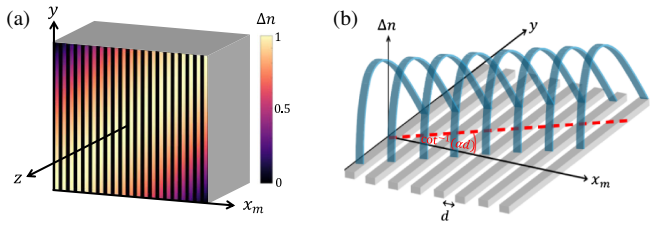

FIG. 1. (a) Sketch of the judiciously shaped slab waveguide lattice in real space, with a refractive index structure of $\Delta n = -(m - \alpha y)^2$. The evanescently coupled waveguides are aligned along the x direction, labeled with the integer m. The refractive index does not depend on the propagation axis z; namely, Δn remains invariant for all z. (b) Side view of the waveguide array (gray) with the shape of the refractive index (blue): Each waveguide has a translated parabolic "effective potential" (refractive index).

introduces considerable coupling to radiation modes, which sets a limit on the propagation distance. Likewise, spatial modulation involves backscattering, and temporal modulation in cavities leads to coupling to low-Q modes. Thus, having PTIs without any modulation makes them appealing for photonic devices.

The photonic structure is based on the fact that the Hamiltonian of a charged particle confined to a plane in the presence of a perpendicular uniform magnetic field is equivalent to a set of harmonic oscillators with shifted centers. Consider a 1D spatial lattice, composed of an array of evanescently coupled planar (slab) waveguides, engraved in a 3D dielectric medium (Fig. 1a). The waveguides have their propagation axis in the z direction, and they are periodically spaced in x by a distance d. The waveguides are labeled with an (integer) index m, such that $-\infty < m < \infty$. The contrast of the refractive index defining the waveguides is varied in the y direction in the form $\Delta n = -(m - \alpha y)^2$. Namely, Δn depends on the waveguide number (m), such that the largest index contrast moves in the x-y plane at an angle $\cot^{-1}(\alpha d)$ [Fig. 1(b)].

The evolution of EM waves in this photonic structure is governed by the paraxial wave equation

$$i\frac{\partial \psi(\boldsymbol{r}, z)}{\partial z} = -\frac{1}{2k_0}\nabla_\perp^2 \psi(\boldsymbol{r}, z) - \frac{k_0}{n_0}\Delta n(\boldsymbol{r}, z)\psi(\boldsymbol{r}, z). \quad (1)$$

This equation is mathematically equivalent to the Schrödinger equation with the coordinate z playing the role of time, and $\Delta n(\boldsymbol{r}, z)/n_0$—the fractional change in the refractive index—acting as the effective potential [40]. $\psi(\boldsymbol{r}, z)$ is the slowly varying envelope of the wave, $k_0 = 2\pi n_0/\lambda$ is the wave number in the medium (λ is the wavelength), n_0 is the ambient refractive index, and $\nabla_\perp^2 = \partial_x^2 + \partial_y^2$ is the Laplacian in the transverse plane (x, y). The equivalence between Eq. (1) and the Schrödinger equation has been exploited in experimenting with a variety of phenomena, from Anderson localization [41] and bound states in the continuum [42] to Floquet TIs in real space [4] and in synthetic dimensions [28]. Thus, with the refractive index structure $\Delta n(x_m, y)$ ($x_m = md$ being the position of the mth waveguide) and under tight binding, Eq. (1) takes the form

$$i\frac{\partial}{\partial z}\varphi_m(y) = \kappa\left(\frac{\varphi_{m+1} + \varphi_{m-1}}{2}\right) + \left[\frac{1}{2k_0}\left(i\frac{\partial}{\partial y}\right)^2 + \frac{k_0}{n_0}(m - \alpha y)^2\right]\varphi_m(y), \quad (2)$$

where φ_m is the wave function in the mth waveguide and κ is the coupling constant between adjacent waveguides. Since φ_m is discrete in x, we can write $\psi = \sum_m \varphi_m(y)e^{ik_x md}$ and express Eq. (2) in a synthetic domain of (k_x, y), where the evolution is described by

$$i\frac{\partial}{\partial z}\psi(k_x, y) = \left[\kappa\cos(k_x d) + \frac{k_0}{n_0}\left(i\frac{1}{d}\frac{\partial}{\partial k_x} - \alpha y\right)^2 + \frac{1}{2k_0}\left(i\frac{\partial}{\partial y}\right)^2\right]\psi(k_x, y), \quad (3)$$

where k_x is the wave number along the x direction. Equation (3) is equivalent to the Schrödinger equation for a charged particle in a magnetic field [36], under

$$i\frac{\partial \psi(\boldsymbol{r}, z)}{\partial t} = \left[\frac{1}{2m}[\hat{p}_x - q\hat{A}_x(y)]^2 + \frac{\hat{p}_y^2}{2m} + qv(\boldsymbol{r})\right]\psi(\boldsymbol{r}, z), \quad (4)$$

$\hbar = c = q = 1$, and using the kinetic momentum operator $\hat{\boldsymbol{p}} = -i\hbar\nabla$. The magnetic field is induced by the term (αy), acting as a vector potential $\boldsymbol{A}_x(y) = \alpha y\hat{x}$ in the (k_x, y) domain. Using this 1D transformation, we obtain an artificial uniform magnetic field, $\boldsymbol{H}_{\text{art}} = -\alpha\hat{z}$, perpendicular to the synthetic-space plane of (k_x, y).

Intuitively, the refractive index $\Delta n = -(m - \alpha y)^2$ means that each waveguide has a parabolic envelope; hence, the structure acts as a system of coupled harmonic oscillators, with the center of each oscillator translated linearly in y, depending on the position of the waveguide index m. In this picture, α is the parameter affecting the curvature of the harmonic potential in each waveguide and the translation in the center of the harmonic potential in y [Fig. 1(b)]. These waveguides (shifted harmonic oscillators) are coupled by proximity. Importantly, this structure is *completely uniform along the z direction*. Namely, this structure is propagation invariant. In the equivalent Schrödinger picture, where z plays the role of time, this means that the *time-reversal symmetry in this system is conserved*. This structure, which is invariant under translations in the propagation axis z, displays dynamics similar to that of a time-independent Hamiltonian: It conserves energy precisely for different z plane cuts; i.e., there is no coupling to unbound modes. Likewise, the z-invariant Hamiltonian also conserves momentum; hence, there is no backreflection.

The topological properties in our system are manifested in synthetic space, which consists of one spatial axis (y) and one synthetic axis of the momentum k_x, obtained by converting a spatial dimension (x) to a synthetic dimension (k_x). Our 2D synthetic space is, therefore, a hybrid real-momentum space. While this transformation does not change the eigenvalues of the problem, it introduces a vector potential $\boldsymbol{A}_x(y)$ of an artificial magnetic field perpendicular to the new transverse coordinates (k_x, y). This effective magnetic field, induced in the synthetic domain, exhibits properties of a quantum Hall effect: In the presence of a uniform magnetic field normal to the plane, the energy spectrum breaks up into discrete Landau levels. In our structure, the light is influenced by this artificial magnetic field perpendicular to the hybrid real-momentum space (k_x, y). Therefore, the spectrum of our 2D system exhibits Landau levels, with spacing between the levels of $\omega_c = \sqrt{2/n_0}\alpha$, the cyclotron frequency (see the derivation in Supplemental Material [43]). We emphasize that the $\kappa\cos(k_x d)$ term in Eq. (3) removes the degeneracy of the Landau plateaus. However, as long as the coupling coefficient remains small, namely, $\kappa < \omega_c$, one can still distinguish between the equally spaced plateaus, even if the shape of the plateaus is somewhat modified. The spectrum of Landau levels can be viewed as the "band structure" of the system, as used henceforth. In our photonic structure, the spectrum is defined by the evolution of the eigenmodes $\psi_n = \varphi_n e^{i\beta z}$, β being the propagation constant. Since the potential in this system does not obey translational symmetry, we arrange the spectrum in ascending values of β, which displays Landau levels [Fig. 2(a)]. When we take our structure to be finite in the y direction, we find (using periodic boundary conditions in y) edge states in the gaps of the Landau levels [inset in Fig. 2(a)]. These edge states are natural candidates for being topological edge modes. Figure 2(b) shows the uniform artificial magnetic field oriented along the $(-z)$ direction.

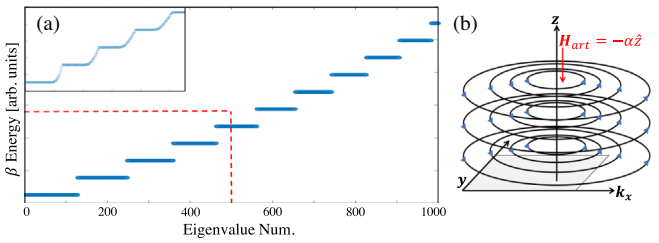

FIG. 2. . (a) Landau level spectrum: propagation constants in ascending order. The eigenvalues congregate at discrete, highly degenerate plateaus, with level spacing conforming to the cyclotron frequency $\omega_c = \sqrt{2/n_0}\alpha$. Λ is an interval of eigenvalues encompassing the first plateaus. Inset: spectrum of the region marked by a dashed red line, when the structure is finite in y. The Landau levels are connected by edge modes. (b) Motion of an eigenstate wave function in synthetic plane (k_x, y). The wave function evolves in an anticlockwise cyclotron motion resembling the motion of a charge in the presence of a uniform magnetic field.

Having shown that our evolution-invariant system has an artificial magnetic field, the immediate question is whether it is topological. Conventionally, the topology of a system is represented by the Chern number, reflecting the winding number accumulated over a full cycle in momentum space. However, since our 2D system is not periodic in its spatial dimensions (x and y), there is no unit cell nor Brillouin zone; hence, we resort to the real-space Chern number [44,45]. As described in Supplemental Material [43], we find the Chern number to be $+1$, indicating that the system has nontrivial topology.

It is important to emphasize again that our topological structure is completely invariant in the z direction. Thus, in the analogous Schrödinger picture, our system of shifted coupled harmonic oscillators is fully time invariant. In our synthetic space, however, time-reversal symmetry is broken. Namely, since our hybrid real-momentum space consists of a momentum dimension k_x and a spatial dimension y, time-reversal symmetry in the synthetic domain is broken, because time-reversal flips the sign of the momentum $T\{\hat{k}_x \times \hat{y}\} = -\hat{k}_x \times \hat{y}$. This is what enables the creation of the artificial magnetic field in the synthetic space.

Next, we study the propagation of wave packets within the bulk and on the edge of the synthetic-space structure using simulations of Eq. (1). We begin with the evolution in the bulk (of synthetic space): We launch a wave packet of the form $\psi(k_x, y) \cdot e^{ivk_x}$, where $\psi(k_x, y)$ is a Gaussian wave packet and v is a real number playing the role of "wave number in synthetic space" (not to be confused with the group velocity; see Supplemental Material [43]). We first launch the wave packet at the center of the bulk with a $v > 0$ and let it evolve in z by solving Eq. (1) numerically. Supplemental Video A [43] shows the evolution. The wave packet moves in a circular motion, with group velocity v_g, in an anticlockwise fashion [as expected from Fig. 2(b)]. The motion direction is determined by the artificial magnetic field, which is determined by α (the shift of the parabolic envelope of the refractive index defining the waveguides). For a given α, the magnetic field is always in the same direction; hence, the circular motion of a wave packet in the bulk is always in the same direction. In our example in Supplemental Video A and in Supplemental Material [43], the beam launched in the bulk always moves anticlockwise regardless of its initial synthetic-space wave number v, even if we launch it with $v < 0$. The anticlockwise motion is in accordance with the positive value Chern number $+1$. Thus, our synthetic-space system features distinct chiral properties: circular motion for any wave packet launched in the bulk, with the rotation direction depending on the direction of the artificial magnetic field. This circular motion in synthetic space—common to all

wave packets launched in the bulk—means that there is no transport in the bulk of our synthetic space—conforming the notion of TIs.

The chirality in the synthetic-space bulk leads to complex behavior in real space. The evolution of the beam in the real space shows that it experiences oscillatory evolution around the y direction (without any motion in the x direction), with some broadening (being a superposition of eigenmodes), but it always returns to the same (mean) position where it was launched, after each cyclotron period. The synthetic-space wave number varies throughout evolution: For a beam launched at $k_x = 0$, the wave number oscillates around 0, whereas for $k_x > 0$ the wave number ascends until reaching π and then returning (via Bragg reflection) from $-\pi$ and starting to ascend again (Supplemental Video B [43]). This dynamics is present as long as $0 < \kappa < \omega_c$.

Next, we study the evolution of a wave packet along the edge, by taking a ribbon in the synthetic domain with a finite width in y. We launch a Gaussian wave packet with synthetic-space wave number $v > 0$ at the upper edge [Figs. 3(a)–3(d) and Supplemental Video C [43]] and with $v < 0$ at the bottom edge [Figs. 3(e)–3(h) and Supplemental Video D [43]] of this ribbon. For the upper edge, the beam propagates in a *unidirectional manner*, from *left to right*, while remaining confined to the edge, without penetrating into the bulk. Likewise, a beam launched at the lower edge with $v < 0$ evolves in the same fashion, only in the opposite direction: unidirectionally from *right to left*, always staying at the bottom edge. We emphasize that the eigenstates comprising the wave packet are associated with the energies in the gaps of the Landau levels spectrum [inset in Fig. 2(a)]. This synthetic-space evolution is exactly the characteristic behavior of the topological quantum Hall effect.

It is important, however, to know how this dynamics looks also in real space, where the evolving beam can be directly imaged. When viewed in real space, the wave packet remains localized at the launch position at all times. Namely, when we launch the wave packet at the lower edge of the synthetic-space ribbon with $k_x > 0$, in real space the wave packet remains at the same position and only the wave number is modified, as can be seen in Supplemental video E [43]. This real-space evolution of the synthetic-space edge modes is completely different from the real-space dynamics of the synthetic-space bulk modes: The cyclotron motion of the bulk modes makes oscillatory evolution along the y direction while maintaining its position only in the x coordinate. That is, the k_x motion in the synthetic space affects the envelope of the wave packet, but its center remains at the same x coordinate value. Altogether, the real-space evolution of wave packets associated with synthetic-space edge modes is highly distinct from that of synthetic-space bulk modes. This is visualized in the simulations presented in Supplemental Video E [43], which serves as an indicator for the dynamics expected in laboratory experiments.

One of the key features of topological insulators is robustness of transport against scattering from defects and disorder. Here, our structure is a synthetic-space TI; hence, the robustness should be tested in synthetic space. As shown in Supplemental Material, Sec. C, and in Supplemental Video H [43], edge wave packets are able to bypass defects without scattering back or into the bulk. This serves as a strong confirmation that our system is indeed a synthetic-space TI. However, for most applications, robustness for synthetic-space defects is less important than robustness against real-space scattering, especially against disorder—which is always inevitable in any physical system. To this end, we study the robustness of the edge transport against scattering disorder in real space. We randomly change the refractive index of several waveguides in our structure and simulate the propagation of wave packets on the synthetic-space edge. As shown in Supplemental Videos F and G [43] (which show the evolution in synthetic space and in real space, respectively), the wave packet remains confined to the synthetic-space edge, without being scattered or without coupling to the bulk

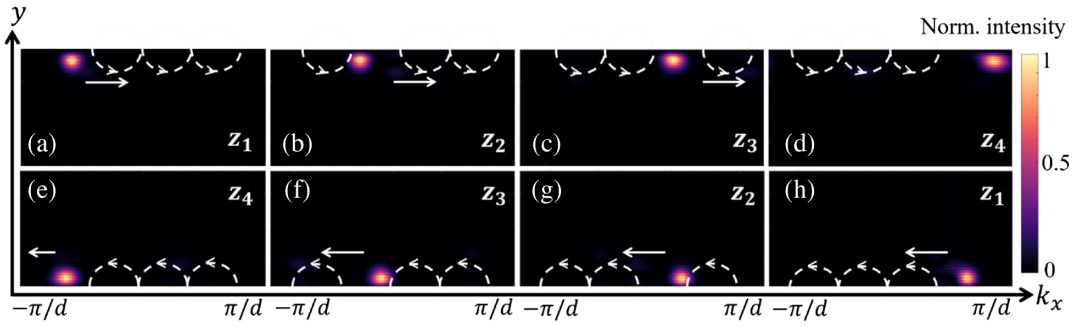

FIG. 3. (a)–(d) Intensity of the beam at four planes in synthetic space. We launch a beam with $v > 0$ at the upper edge of a synthetic-space ribbon. The beam follows the edge from left to right, without scattering into the bulk. (e)–(h) The same as (a)–(d), but with $v < 0$ at the lower edge of the synthetic-space ribbon, displaying evolution from right to left. We use the parameters $d = 12.566$ [μm], $\lambda = 0.5236$ [μm], and $\alpha = 12.5664$ [cm^{-1}]. The y values vary between -125 and 125 [μm].

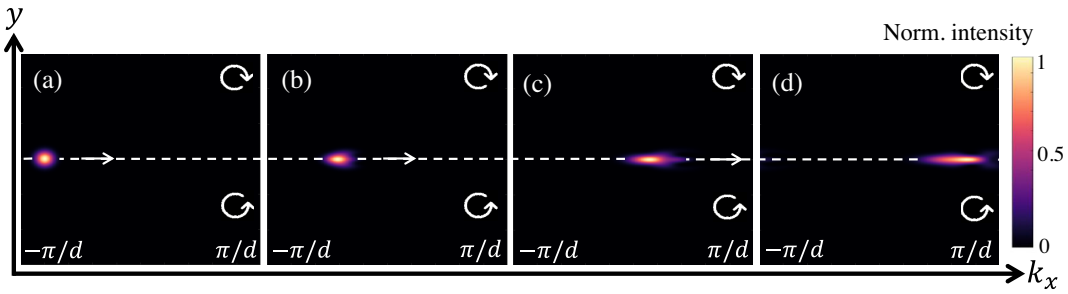

FIG. 4. (a)–(d) Evolution of a beam launched with $v > 0$ along the interface between the two systems with opposite chiralities. The beam propagates unidirectionally without coupling into the bulks. The parameters are the same as in Fig. 3.

modes—even when we increase the magnitude of the disorder, as long as it is smaller than the half of our band gap.

Finally, we explore the evolution of the edge states at the $y = 0$ interface between two systems of opposite chirality and launch a wave packet with $v > 0$ along this interface. For $y > 0$, the bulk has a refractive index $\Delta n_1 = -(m + \alpha y)^2$, and, for $y < 0$, the bulk has $\Delta n_2 = -(m - \alpha y)^2$. Namely, the bulk with positive y has artificial magnetic field $\boldsymbol{H}_{\text{art}} = +\alpha\hat{z}$, while the adjacent bulk has the opposite artificial magnetic field $\boldsymbol{H}_{\text{art}} = -\alpha\hat{z}$. Thus, the $y = 0$ line signifies an interface between a region with Chern number $+1$ and a region with Chern number -1. As such, the edge states at this interface correspond to a difference in the Chern number of 2, which implies that their dispersion relation and wave functions are fundamentally different than those in Fig. 3 (where the interfacial change in Chern number was 1). The Chern number also dictates the number of chiral edge states residing at the interface of the coupled structures. The spectrum of these coupled structures is presented in Supplemental Material [43]. Figures 4(a)–4(d) and Supplemental Video I [43] show the simulated dynamics of a beam (made up of the proper edge states) launched with $v > 0$ at this topological interface of difference in the Chern number of 2. The beam remains confined to the interface throughout propagation, without coupling into any of the bulks. On the other hand, when we launch the same wave packet but with $v < 0$, which is opposite to the direction of the one-way propagation induced by the chiralities of the two coupled bulks, the beam remains at the same (mean) position where it was launched. The beam splits in two, each half making circular motion in the chiral direction of its bulk (Supplemental Material and Supplemental Video J [43]).

In conclusion, we proposed an evolution-invariant 2D structure which is a synthetic-space TI. This structure is the first evolution-invariant topological insulator in a bosonic wave system. It is characterized by an artificial magnetic field displaying Landau levels and a positive Chern number $+1$, even though time-reversal symmetry is not broken in real space. Accordingly, the topological edge states in this structure move unidirectionally in the hybrid real-momentum space, without scattering into the bulk or backscattering, even in the presence of real-space disorder. This evolution-invariant TI, which does not require any kind of modulation, makes it appealing to experiments in photonics (as described above) and in cold atom systems (where laser beams induce a 1D lattice superimposed with parabolic envelopes of translated centers, as in Fig. 1). These would be the first experimental realization of an evolution-invariant TI in synthetic dimensions, highlighting a fundamentally new mechanism for TIs that creates chiral edge states without breaking time-reversal symmetry in their real space.

Note added.—Recently, a related work appeared [47], demonstrating a similar structure to ours—also evolution invariant, which exhibits chiral edge states.

This work was supported by an Advanced Grant from the European Research Council (ERC) under the European Union's Horizon 2020 research and innovation programme (Grant agreement No 789339), by the US Air Force Office for Science Research (AFOSR), and by the Israel Science Foundation.

*msegev@technion.ac.il

[1] M. Z. Hasan and C. L. Kane, Colloquium: Topological insulators, Rev. Mod. Phys. **82**, 3045 (2010).
[2] M. König, S. Wiedmann, C. Brüne, A. Roth, H. Buhmann, L. W. Molenkamp, X. L. Qi, and S. C. Zhang, Quantum spin Hall insulator state in HgTe quantum wells, Science **318**, 766 (2007).
[3] Z. Wang, Y. Chong, J. D. Joannopoulos, and M. Soljačić, Observation of unidirectional backscattering-immune topological electromagnetic states, Nature (London) **461**, 772 (2009).
[4] M. C. Rechtsman, J. M. Zeuner, Y. Plotnik, Y. Lumer, D. Podolsky, F. Dreisow, S. Nolte, M. Segev, and A. Szameit, Photonic floquet topological insulators, Nature (London) **496**, 196 (2013).
[5] M. Hafezi, S. Mittal, J. Fan, A. Migdall, and J. M. Taylor, Imaging topological edge states in silicon photonics, Nat. Photonics **7**, 1001 (2013).
[6] F. Gao, Z. Gao, X. Shi, Z. Yang, X. Lin, H. Xu, J. D. Joannopoulos, M. Soljačić, H. Chen, L. Lu, and Y. Chong,

Probing topological protection using a designer surface plasmon structure, Nat. Commun. **7**, 11619 (2016).
[7] K. Lai, T. Ma, X. Bo, S. Anlage, and G. Shvets, Experimental realization of a reflections-free compact delay line based on a photonic topological insulator, Sci. Rep. **6**, 28453 (2016).
[8] X. Wu, Y. Meng, J. Tian, Y. Huang, H. Xiang, D. Han, and W. Wen, Direct observation of valley-polarized topological edge states in designer surface plasmon crystals, Nat. Commun. **8**, 1304 (2017).
[9] T. Ozawa, H. M. Price, A. Amo, N. Goldman, M. Hafezi, L. Lu, M. C. Rechtsman, D. Schuster, J. Simon, O. Zilberberg, and I. Carusotto, Topological photonics, Rev. Mod. Phys. **91**, 015006 (2019).
[10] G. Jotzu, M. Messer, R. Desbuquois, M. Lebrat, T. Uehlinger, D. Greif, and T. Esslinger, Experimental realization of the topological Haldane model with ultracold fermions, Nature (London) **515**, 237 (2014).
[11] M. Aidelsburger, M. Lohse, C. Schweizer, M. Atala, J. T. Barreiro, S. Nascimbène, N. R. Cooper, I. Bloch, and N. Goldman, Measuring the Chern number of Hofstadter bands with ultracold bosonic atoms, Nat. Phys. **11**, 162 (2015).
[12] C. He, X. Ni, H. Ge, X. C. Sun, Y. Bin Chen, M. H. Lu, X. P. Liu, and Y. F. Chen, Acoustic topological insulator and robust one-way sound transport, Nat. Phys. **12**, 1124 (2016).
[13] Z. Yang, F. Gao, X. Shi, X. Lin, Z. Gao, Y. Chong, and B. Zhang, Topological Acoustics, Phys. Rev. Lett. **114**, 114301 (2015).
[14] S. Roman and D. H. Sebastian, Observation of phononic helical edge states in a mechanical topological insulator, Science **349**, 47 (2015).
[15] S. D. Huber, Topological mechanics, Nat. Phys. **12**, 621 (2016).
[16] L. Lu, J. D. Joannopoulos, and M. Soljačić, Topological photonics, Nat. Photonics **8**, 821 (2014).
[17] M. Segev and M. A. Bandres, Topological photonics: Where do we go from here?, Nanophotonics **10**, 425 (2020).
[18] T. Ma, A. B Khanikaev, S. H. Mousavi, and G. Shvets, Guiding Electromagnetic Waves Around Sharp Corners: Topologically Protected Photonic Transport in Metawaveguides, Phys. Rev. Lett. **114**, 127401 (2015).
[19] G. Harari, M. A. Bandres, Y. Lumer, M. C. Rechtsman, Y. D. Chong, M. Khajavikhan, D. N. Christodoulides, and M. Segev, Topological insulator laser: Theory, Science **359**, eaar4003 (2018).
[20] A. Celi, P. Massignan, J. Ruseckas, N. Goldman, I. B. Spielman, G. Juzeliunas, and M. Lewenstein, Synthetic Gauge Fields in Synthetic Dimensions, Phys. Rev. Lett. **112**, 043001 (2014).
[21] M. Mancini, G. Pagano, G. Cappellini, L. Livi, M. Rider, J. Catani, C. Sias, P. Zoller, M. Inguscio, M. Dalmonte, and L. Fallani, Observation of chiral edge states with neutral fermions in synthetic Hall ribbons, Science **349**, 1510 (2015).
[22] B. K. Stuhl, H. I. Lu, L. M. Aycock, D. Genkina, and I. B. Spielman, Visualizing edge states with an atomic Bose gas in the quantum Hall regime, Science **349**, 1514 (2015).
[23] F. A. An, E. J. Meier, and B. Gadway, Direct observation of chiral currents and magnetic reflection in atomic flux lattices, Sci. Adv. **3**, e1602685 (2017).
[24] L. Yuan, Y. Shi, and S. Fan, Photonic gauge potential in a system with a synthetic frequency dimension, Opt. Lett. **41**, 741 (2016).
[25] T. Ozawa, H. M. Price, N. Goldman, O. Zilberberg, and I. Carusotto, Synthetic dimensions in integrated photonics: From optical isolation to four-dimensional quantum Hall physics, Phys. Rev. A **93**, 043827 (2016).
[26] X. W. Luo, X. Zhou, C. F. Li, J. S. Xu, G. C. Guo, and Z. W. Zhou, Quantum simulation of 2D topological physics in a 1D array of optical cavities, Nat. Commun. **6**, 7704 (2015).
[27] A. Dutt, Q. Lin, L. Yuan, M. Minkov, M. Xiao, and S. Fan, A single photonic cavity with two independent physical synthetic dimensions, Science **367**, 59 (2020).
[28] E. Lustig, S. Weimann, Y. Plotnik, Y. Lumer, M. A. Bandres, A. Szameit, and M. Segev, Photonic topological insulator in synthetic dimensions, Nature (London) **567**, 356 (2019).
[29] D. Jukić and H. Buljan, Four-dimensional photonic lattices and discrete tesseract solitons, Phys. Rev. A **87**, 013814 (2013).
[30] Y. E. Kraus, Z. Ringel, and O. Zilberberg, Four-Dimensional Quantum Hall Effect in a Two-Dimensional Quasicrystal, Phys. Rev. Lett. **111**, 226401 (2013).
[31] O. Zilberberg, S. Huang, J. Guglielmon, M. Wang, K. P. Chen, Y. E. Kraus, and M. C. Rechtsman, Photonic topological boundary pumping as a probe of 4D quantum Hall physics, Nature (London) **553**, 59 (2018).
[32] A. L. M. Muniz, A. Alberucci, C. P. Jisha, M. Monika, S. Nolte, R. Morandotti, and U. Peschel, Kapitza light guiding in photonic mesh lattice, Opt. Lett. **44**, 6013 (2019).
[33] H. M. Price, T. Ozawa, and N. Goldman, Synthetic dimensions for cold atoms from shaking a harmonic trap, Phys. Rev. A **95**, 023607 (2017).
[34] E. Lustig and M. Segev, Topological photonics in synthetic dimensions, Adv. Opt. Photon. **13**, 426 (2021).
[35] H. M. Price, T. Ozawa, and I. Carusotto, Quantum Mechanics with a Momentum-Space Artificial Magnetic Field, Phys. Rev. Lett. **113**, 190403 (2014).
[36] These results were first presented in L. Nemirovsky, M.-I. Cohen, Y. Lumer, E. Lustig, and M. Segev, Magnetic gauge field for photons in synthetic dimensions by a propagation-invariant photonic structure, in *Conference on Lasers Electro-Optics, OSA Technical Digest (Optical Society of America)* (2019), paper FW3D.7; More advanced results were presented a year later: L. Nemirovsky, M.-I. Cohen, Y. Lumer, E. Lustig, and M. Segev, Topological evolution-invariant photonic structures in synthetic dimensions, in *Conference on Lasers Electro-Optics, OSA Technical Digest (Optical Society of America)* (2020), paper FW4A.1.
[37] H. M. Price, O. Zilberberg, T. Ozawa, I. Carusotto, and N. Goldman, Four-Dimensional Quantum Hall Effect with Ultracold Atoms, Phys. Rev. Lett. **115**, 195303 (2015).
[38] Z. Yang, E. Lustig, G. Harari, Y. Plotnik, Y. Lumer, M. A. Bandres, and M. Segev, Mode-Locked Topological Insulator Laser Utilizing Synthetic Dimensions, Phys. Rev. X **10**, 011059 (2020).
[39] D. Marcuse, Loss analysis of single-mode fiber splices, Bell Syst. Tech. J. **56**, 703 (1977).
[40] F. Lederer, G. I. Stegeman, D. N. Christodoulides, G. Assanto, M. Segev, and Y. Silberberg, Discrete solitons in optics, Phys. Rep. **463**, 1 (2008).

[41] T. Schwartz, G. Bartal, S. Fishman, and M. Segev, Transport and Anderson localization in disordered two-dimensional photonic lattices, Nature (London) **446**, 52 (2007).

[42] Y. Plotnik, O. Peleg, F. Dreisow, M. Heinrich, S. Nolte, A. Szameit, and M. Segev, Experimental Observation of Optical Bound States in the Continuum, Phys. Rev. Lett. **107**, 183901 (2011).

[43] See Supplemental Material at http://link.aps.org/supplemental/10.1103/PhysRevLett.127.093901 for more details about the real-space Chern number and the structure and additional features of it which includes Refs. [44–46].

[44] A. Kitaev, Anyons in an exactly solved model and beyond, Ann. Phys. (Amsterdam) **321**, 2 (2006).

[45] N. P. Mitchell, L. M. Nash, D. Hexner, A. M. Turner, and W. T. M. Irvine, Amorphous topological insulators constructed from random point sets, Nat. Phys. **14**, 380 (2018).

[46] Z. Yang, E. Lustig, Y. Lumer, and M. Segev, Photonic Floquet topological insulators in a fractal lattice, Light Sci. Appl. **9**, 128 (2020).

[47] T. Ozawa, Artificial magnetic field for synthetic quantum matter without dynamical modulation, Phys. Rev. A **103**, 033318 (2021).